Electronic Supplementary Material (ESI) for Journal of Materials Chemistry C.

Supporting Information

Lead-free Mn^{II}-based Red-emitting Hybrid Hahide $(CH_6N_3)_2MnCl_4$ toward High Performance Warm WLEDs

Shiyi Wang,[a] Xinxin Han,*[a] Tongtong Kou,[a] Yayun Zhou,[b] Yi Liang,[a] Zixuan Wu,[a] Jialuo Huang,[a] Tong Chang,[a] Chengyu Peng,[a] Qilin Wei,[a] Bingsuo Zou*[a]

[a] *School of Physical Science and Technology, MOE Key Laboratory of New Processing Technology for Non-ferrous Metals and Materials, Guangxi Key Laboratory of Processing for Non-ferrous Metals and Featured Materials, Guangxi University, Nanning 530004, China.*

[b] *State Key Laboratory of Luminescent Materials and Devices, Guangdong Provincial Key Laboratory of Fiber Laser Materials and Applied Techniques, South China University of Technology, Guangzhou 510641, China.*

Experimental section

Materials and Chemicals

The raw materials manganese(II) chloride tetrahydrate ($MnCl_2{\cdot}4H_2O$, 99%, Aladdin), guanidine hydrochloride (CH_6N_3Cl, AR, Xilong Chemical Co., Ltd., China), zinc chloride ($ZnCl_2$, 99.0%, Aladdin), hydrochloric acid (HCl, 36−38wt.% in water, Beijing Chemical Works), and absolute ethanol (AR, Beijing Tongguang Fine Chemical Co., Ltd., China) were purchased and used as received without further purification.

Synthesis

The polycrystalline samples $(CH_6N_3)_2MnCl_4$ and Zn^{2+}-doped $(CH_6N_3)_2MnCl_4$ were synthesized by a facile mechanochemical method through manual grinding in an agate mortar. For the preparation of $(CH_6N_3)_2MnCl_4$, 1 mmol $MnCl_2{\cdot}4H_2O$ and 2 mmol of CN_3H_6Cl were put into an agate mortar and ground with a pestle. The powder rapidly exhibited red fluorescence with continuous grinding under the irradiation of 365 nm ultraviolet (UV) lamp. In order to ensure the complete reaction of raw materials, the powder was thoroughly ground for several minutes. The Zn^{2+} doped samples were prepared by the similar procedure besides the addition of certain amount of $ZnCl_2$ to replace the same amount of $MnCl_2·4H_2O$.

Fabrication of WLEDs

WLEDs were fabricated by combining high-power COB blue InGaN chips (~450 nm, 300 mA, 10 W), commercial $Y_3Al_5O_{12}:Ce^{3+}$ ($YAG:Ce^{3+}$) yellow phosphor and the as-prepared $(CH_6N_3)_2MnCl_4$ or $(CN_3H_6)_2Mn_{0.92}Zn_{0.08}Cl_4$ phosphor. The phosphors were mixed with epoxy resin thoroughly, and coated on the surface of the COB chips to produce WLEDs.

Measurement and Characterization

Room-temperature (RT) X-ray Diffraction (XRD) measurements were carried out using a SMARTLAB 3KW Diffractometer with Cu Kα (λ =1.5406 Å) radiation. The Rietveld method was employed to perform the structure refinement by program General Structure Analysis System (GSAS).[1] Temperature-dependent XRD spectra were carried out on a Bruker D8 Diffractometer in the temperature range of 140-360 K with an interval of 20 K. Raman spectra were carried out using WITec alpha300R Raman spectrometer with a 325 nm laser. The thermal stability of the sample was measured on a differential thermogravimetric (TGA) analyzer (DTG-60H) from RT to 800°C under nitrogen atmosphere. The morphology and elemental composition were performed using a field emission scanning electron microscope (SEM, Sigma 500) equipped with energy dispersive X-ray spectroscopy (EDS). The photoluminescence excitation (PLE), photoluminescence (PL) spectra, PL decay curves and PL quantum yields (PLQYs) were measured by a Horiba Jobin Yvon Fluorolog-3 fluorescence spectrophotometer equipped with a 450 W Xenon lamp or a μs flash lamp as the excitation source as well as the high and low temperature test system. The absorption spectra were measured by UV-vis spectrophotometer (PerkinElmer Instruments, Lambda 750). The upconversion spectrum was recorded on an Edinburgh FLS1000 fluorescence spectrometer equipped with a 980 nm femtosecond laser. The magnetic property was measured by a vibration sample magnetometer (VSM) (Lakeside,7410). The photoelectric properties of the as-fabricated pc-WLEDs, including the EL spectrum, luminous efficacy (LE), color rendering index (CRI), correlated color temperature (CCT), and Commission Internationale de L'Eclairage (CIE) chromaticity coordinate, were measured using a ATA-1000 (Everfine, China) opto-electronic analyzer.

Table S1 Rietveld refinement data for $(CH_6N_3)_2MnCl_4$.

formula	$(CH_6N_3)_2MnCl_4$
space group	$P2_1/c$
a (Å)	8.66306(18)
b (Å)	27.07211(20)
c (Å)	15.63008(17)
α (°)	90
β (°)	93.1929(20)
γ (°)	90
Z	12
V ($Å^3$)	3659.99(9)
R_{wp} (%)	5.45
R_p (%)	4.19
χ^2	1.607

Note: The refinements are stable and give low R-factors.

Table S2 Average bond lengths (Å) and distortion index of $MnCl_6$ octahedron in $(CH_6N_3)_2MnCl_4$

bond	bond length (Å)
Mn1-Cl1	2.257(12)
Mn1-Cl2	2.593(11)
Mn1-Cl3	2.506(12)
Mn1-Cl4	2.816(12)
Mn1-Cl5	2.987(11)
Mn1-Cl6	2.721(10)
Mn2-Cl4	2.528(13)
Mn2-Cl5	2.505(12)
Mn2-Cl6	2.695(12)
Mn2-Cl7	2.737(12)
Mn2-Cl8	2.584(12)
Mn2-Cl9	2.720(14)
Mn3-Cl7	2.856(11)
Mn3-Cl8	2.823(11)
Mn3-Cl9	2.706(13)
Mn3-Cl10	2.665(12)
Mn3-Cl11	2.505(9)
Mn3-Cl12	2.485(13)
average bond lengths (Å)	**2.6494**
distortion index	**0.05167**

The distortion index of the $MnCl_6$ octahedron is calculated by using the following equation [2]:

$$D = \frac{1}{n}\sum_{i=1}^{n}\frac{|l_i - l_{av}|}{l_{av}}$$

where l_i is the distance from the central atom to the ith coordinating atom and l_{av} is the average bond length.

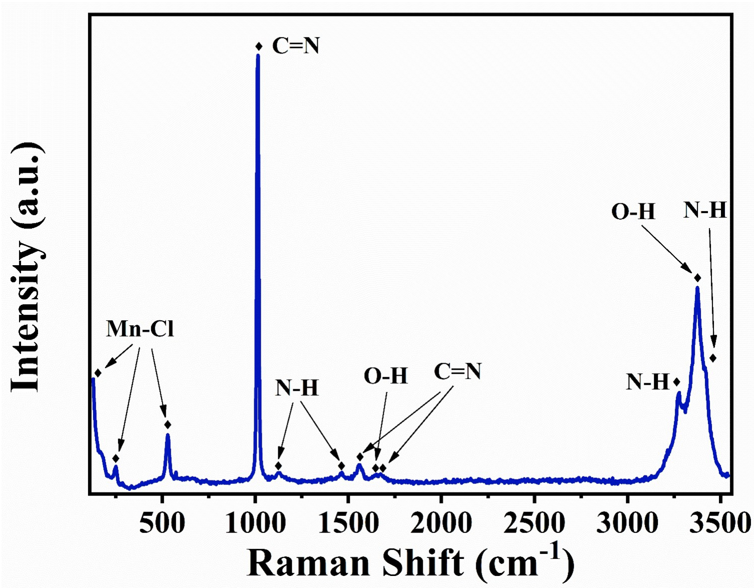

Fig. S1 Raman spectrum of $(CH_6N_3)_2MnCl_4$.

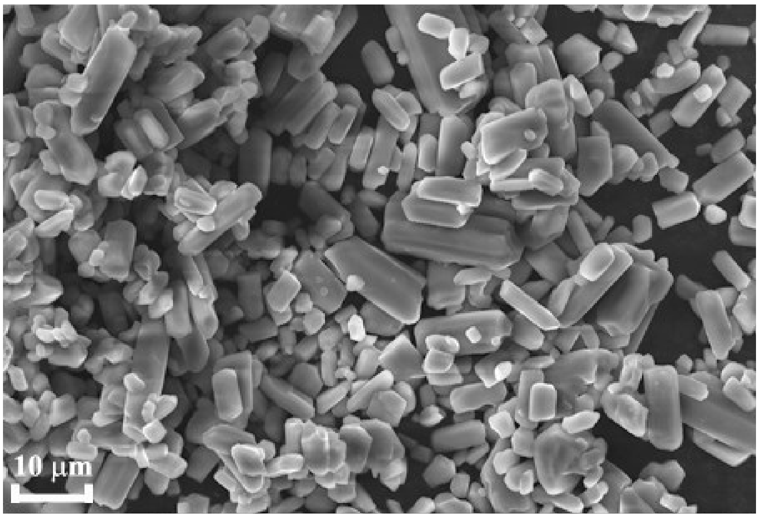

Fig. S2 SEM image of $(CH_6N_3)_2MnCl_4$ powder crystal.

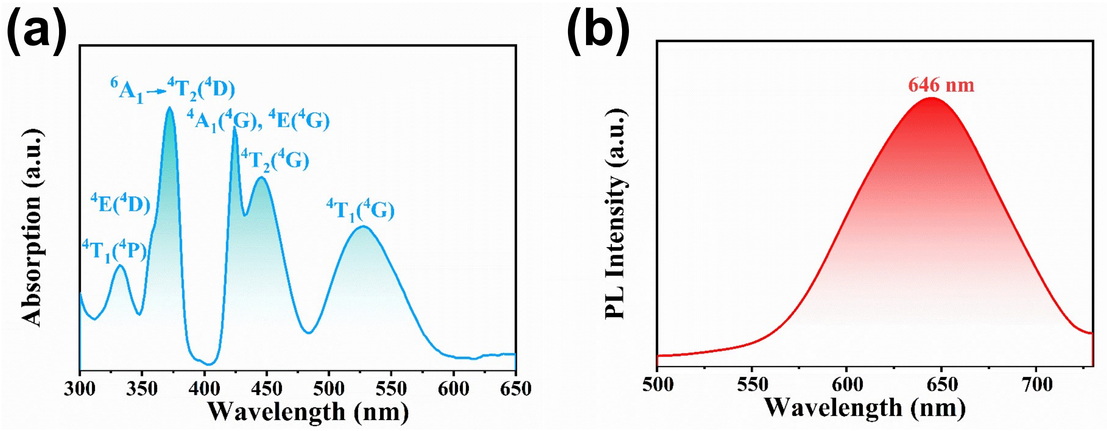

Fig. S3 (a) Absorption spectrum of $(CH_6N_3)_2MnCl_4$. (b) Upconversion spectrum of $(CH_6N_3)_2MnCl_4$ upon excitation of 980 nm femtosecond laser.

Table S3 Luminescent parameters of some reported Mn^{2+}-based halides.

Chemical formula	Peak position (nm)	Lifetime	PLQY	Ref.
$(C_{10}H_{16}N)_2Zn_{1-x}Mn_xBr_4$	518	0.33 ms	0-88.75%	Ref.[3]
(Pyrrolidinium)MnBr	640	157 μs	—	Ref.[4]
(Pyrrolidinium)$MnCl_3$	640	515 μs	53.6%	Ref.[5]
$[(CH_2)_4N(CH_2)_4]_2[MnBr_4]$	525	—	13.07%	Ref.[6]
$[(CH_3)_3NH]_3(MnBr_3)(MnBr_4)$	507, 609	281.7 μs	41.96%	Ref.[7]
$C_4H_{10}NMnBr_3$	628	1.44 ns	46%	Ref.[8]
$C_8H_{20}N_2MnBr_4$	520	3.97 ns	19%	Ref.[8]
$C_5H_6NMnCl_5 \cdot H_2O$	518	1.49 ns	—	Ref.[9]
$C_{10}H_{12}N_2MnCl_4$	620	2.14 ns	—	Ref.[9]
$C_{10}H_{12}N_2MnBr_4$	523	213 μs	—	Ref.[10]
$C_5H_6NMnBr_3$	650	—	—	Ref.[10]
DBFDPO-$MnBr_2$	550	1 ms	81.4%	Ref.[11]
DBFDPO-$MnCl_2$	532	5.3 ms	33.3%	Ref.[11]
(3-Pyrrolinium)$MnCl_3$	635	333.6 μs	28.22%	Ref.[12]
$[(C_7H_{10}N)_2][MnCl_4]$	520	384.43 μs	82%	Ref.[13]
$[(C_7H_{10}N)_2][MnBr_4]$	515	187.83 μs	12%	Ref.[13]
$(Bz(Me)_3N)_2MnX_4$ (X = Cl, Br, I)	500-550	72-380 μs	70-90%	Ref.[14]
$C_4H_{12}NMnCl_3$	635	758.95 μs	91.8%	Ref.[15]
$(C_8H_{20}N)_2MnBr_4$	515	442.52 μs	85.1%	Ref.[15]
Cs_3MnBr_5	520	0.29 ms	49%	Ref.[16]
$(C_6H_{16}N)_2MnBr_4$	525	1.44 ns	62.2%	Ref.[17]
$(C_9H_{20}N)_2MnBr_4$	528	325.57 μs	81.08%	Ref.[18]
$(C_{24}H_{20}P)_2MnBr_4$	522	317 μs	98%	Ref.[19]

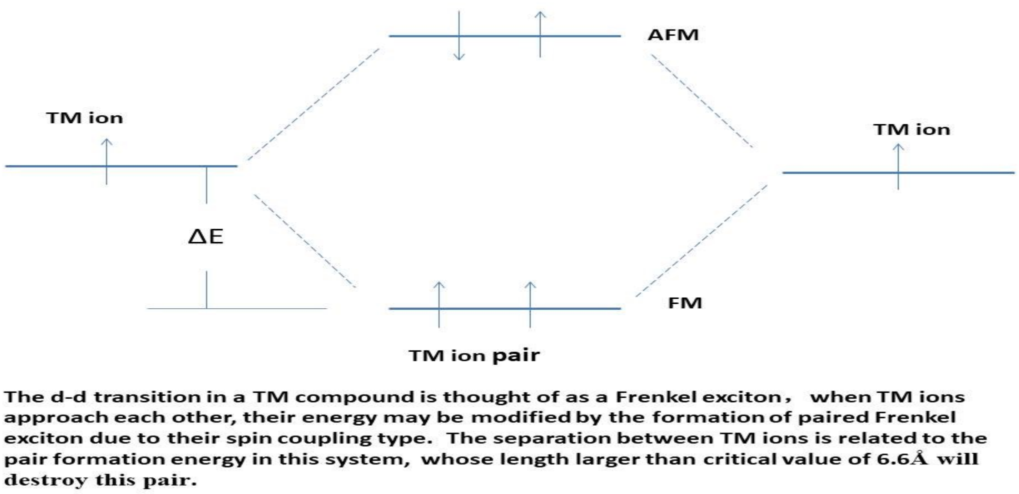

Fig. S4 The spin-spin interaction between transition metal(TM) ion in a TM compound and their d-d transition energy. The ΔE above is the energy E_{sc} of spin-spin coupling between TM ions, whose value is .

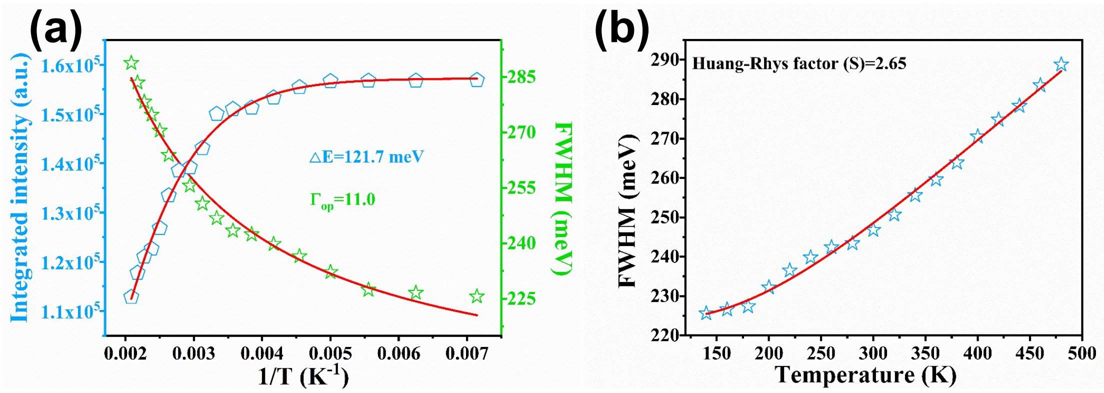

Fig. S5 (a) Integrated intensity and FWHM and the corresponding fitting curves versus temperature. For the integrated intensity, the activation energy ΔE is calculated by fitting the formula of $I_T = I_0 / (1 + \mathrm{A}e^{-\Delta E/kT})$, where A is a constant, k is the Boltzmann constant. For FWHM, the electron-optical phonon coupling energy Γop is calculated by fitting the formula of $\Gamma(\mathrm{T}) = \Gamma_0 + \Gamma_{op} / (e^{\hbar\omega/kT} - 1)$, where Γ0 is the intrinsic line width at absolute temperature 0 K, ħω is the maximum phonon energy. (b) Fitting curve of the FWHM as a function of temperature via the formula of $FWHM(T) = \sqrt{8\ln 2} \times \hbar\omega \times \sqrt{S} \times \sqrt{\coth(\hbar\omega / 2kT)}$ to obtain the Huang-Phys factor S.

Table S4 Photometric and Chromaticity parameters of the fabricated WLEDs.

Device	Current (mA)	CIE coordinates		CCT (K)	Ra	Efficacy (lm/W)
		X	Y			
LED-1 (0%Zn)	20	0.3811	0.3693	3925	94.1	67.56
	60	0.3801	0.3665	3930	94.3	67.83
	120	0.3800	0.3669	3936	95	67.41
	180	0.3808	0.3684	3926	95.5	65.7
	240	0.3806	0.3689	3934	95.7	63.87
	300	0.3806	0.3694	3939	95.9	61.23
LED-2 (8%Zn)	20	0.3784	0.3673	3984	93.7	91.41
	60	0.3802	0.3695	3952	94.1	89.14
	120	0.3820	0.3718	3919	94.4	83.98
	180	0.3839	0.3740	3886	94.3	79.40
	240	0.3861	0.3766	3848	94.1	74.57
	300	0.3875	0.3785	3825	93.9	70.19
LED-3 (0%Zn)	20	0.3392	0.3360	5193	96	96.07
	60	0.3399	0.3373	5166	96.3	94.37
	120	0.3408	0.3388	5135	96.4	89.25
	180	0.3415	0.3402	5108	96.2	84.81
	240	0.3420	0.3413	5089	95.9	80.56
	300	0.3422	0.3418	5084	95.7	76.59
LED-4 (8%Zn)	20	0.3409	0.3408	5132	95.1	107.49
	60	0.3416	0.3417	5110	95.3	104.78
	120	0.3426	0.3431	5070	95.2	99.28
	180	0.3432	0.3439	5048	95.1	94.16
	240	0.3439	0.3448	5023	94.9	89.31
	300	0.3447	0.3459	4996	94.7	84.58
LED-5 (0%Zn)	20	0.3181	0.3371	6175	89.6	120.12
	60	0.3185	0.3377	6154	89.5	117.73
	120	0.3192	0.3388	6114	89.2	111.50
	180	0.3198	0.3398	6083	88.8	105.87
	240	0.3201	0.3404	6067	88.5	100.28
	300	0.3201	0.3402	6067	88.5	94.81
LED-6 (8%Zn)	20	0.3184	0.3347	6175	92.4	122.98
	60	0.3206	0.3380	6049	92	121.44
	120	0.3229	0.3411	5931	91.5	119.9
	180	0.3247	0.3436	5843	90.9	108.94
	240	0.3263	0.3460	5769	90.4	102.94
	300	0.3283	0.3487	5680	89.8	96.69

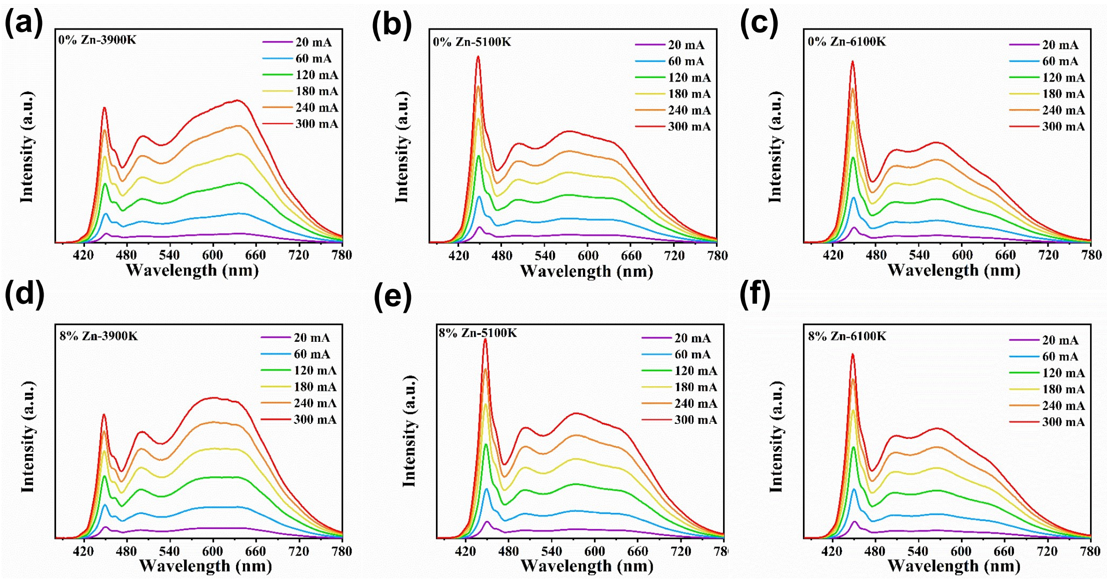

Fig. S6 Drive current dependent electroluminescence spectra of WLED devices with different CCT fabricated with the as-synthesized red-emitting hybrid halides $(CH_6N_3)_2MnCl_4$ or $(CH_6N_3)_2MnCl_4$:8%Zn^{2+} and the commercial yellow phosphor YAG:Ce^{3+} on a blue InGaN chip: (a-c) WLED devices fabricated by $(CH_6N_3)_2MnCl_4$ with CCT of ~3900, 5100 and 6100 K, respectively. (d-f) WLED devices fabricated by $(CH_6N_3)_2MnCl_4$:8%Zn^{2+} with CCT of ~3900, 5100 and 6100 K, respectively.

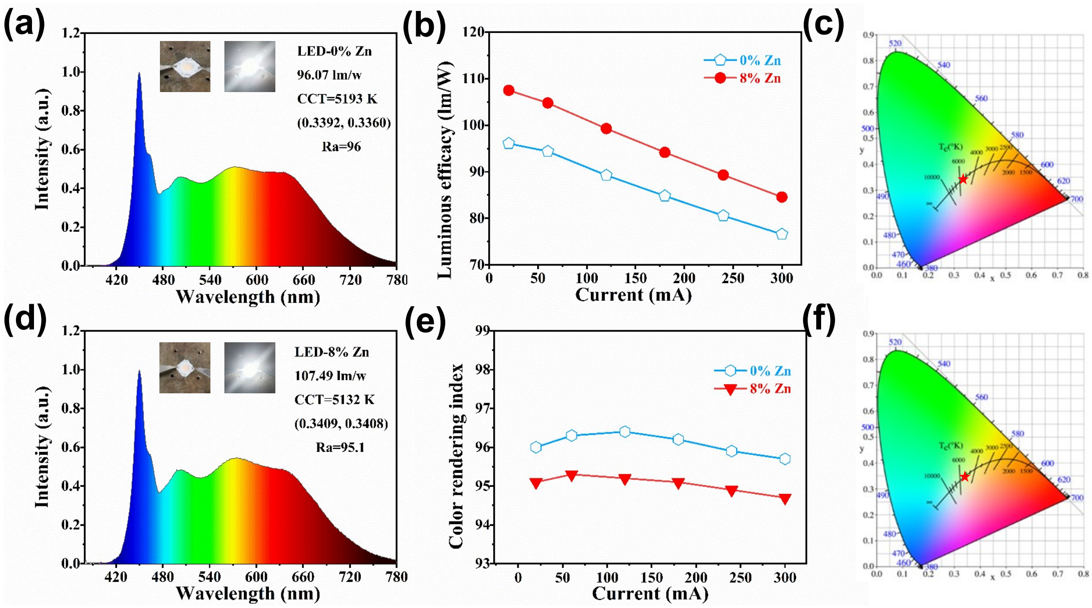

Fig. S7 (a and d) Electroluminescence spectra of the WLED devices with CCT of ~5100 K fabricated with the as-synthesized red-emitting hybrid halides $(CH_6N_3)_2MnCl_4$, $(CH_6N_3)_2MnCl_4$:8%Zn^{2+} and the commercial yellow phosphor YAG:Ce^{3+} on a blue InGaN chip under a driven current of 20 mA, respectively. The inset shows the photographs of the as-fabricated and lightened WLED. (b) Comparison of drive current dependent luminous efficacy of the WLEDs fabricated by $(CH_6N_3)_2MnCl_4$ and $(CH_6N_3)_2MnCl_4$:8%Zn^{2+}. (e) Comparison of drive current dependent color rendering index of the WLEDs fabricated by $(CH_6N_3)_2MnCl_4$ and $(CH_6N_3)_2MnCl_4$:8%Zn^{2+}. (c and f) CIE chromaticity coordinates of the WLEDs fabricated by $(CH_6N_3)_2MnCl_4$ and $(CH_6N_3)_2MnCl_4$:8%Zn^{2+}, respectively.

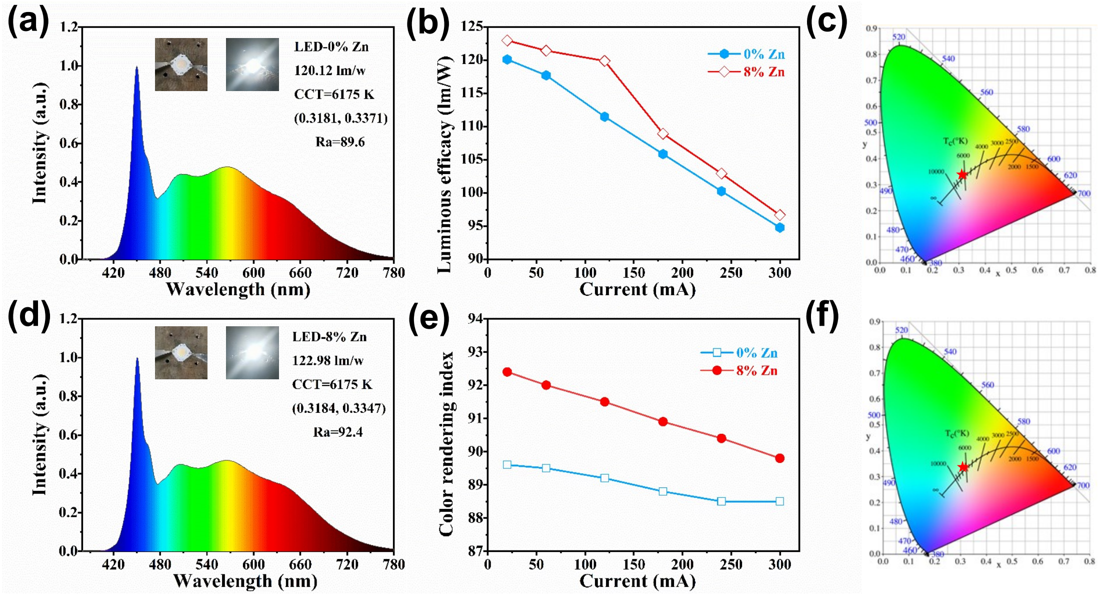

Fig. S8 (a and d) Electroluminescence spectra of the WLED devices with CCT of ~6100 K fabricated with the as-synthesized red-emitting hybrid halides $(CH_6N_3)_2MnCl_4$, $(CH_6N_3)_2MnCl_4$:8%Zn^{2+} and the commercial yellow phosphor YAG:Ce^{3+} on a blue InGaN chip under a driven current of 20 mA, respectively. The inset shows the photographs of the as-fabricated and lightened WLED. (b) Comparison of drive current dependent luminous efficacy of the WLEDs fabricated by $(CH_6N_3)_2MnCl_4$ and $(CH_6N_3)_2MnCl_4$:8%Zn^{2+}. (e) Comparison of drive current dependent color rendering index of the WLEDs fabricated by $(CH_6N_3)_2MnCl_4$ and $(CH_6N_3)_2MnCl_4$:8%Zn^{2+}. (c and f) CIE chromaticity coordinates of the WLEDs fabricated by $(CH_6N_3)_2MnCl_4$ and $(CH_6N_3)_2MnCl_4$:8%Zn^{2+}, respectively.

References

1. B. H. Toby, *J. Appl. Cryst.*, 2001, **34**, 210-213.
2. J. Qiao, L. Ning, M. S. Molokeev, Y.-C. Chuang, Q. Zhang, K. R. Poeppelmeier and Z. Xia, *Angew. Chem. Int. Ed.*, 2019, **58**, 11521-11526.
3. G. Zhou, Z. Liu, J. Huang, M. S. Molokeev, Z. Xiao, C. Ma and Z. Xia, *J. Phys. Chem. Lett.*, 2020, **11**, 5956-5962.
4. Y. Zhang, W. Q. Liao, D. W. Fu, H. Y. Ye, C. M. Liu, Z. N. Chen and R. G. Xiong, *Adv. Mater.*, 2015, **27**, 3942-3946.
5. Y. Zhang, W. Q. Liao, D. W. Fu, H. Y. Ye, Z. N. Chen and R. G. Xiong, *J. Am. Chem. Soc.*, 2015, **137**, 4928-4931.
6. L. Xu, J. X. Gao, X. G. Chen, X. N. Hua and W. Q. Liao, *Dalton Trans.*, 2018, **47**, 16995-17003.
7. Z. Wei, W. Q. Liao, Y. Y. Tang, P. F. Li, P. P. Li, H. Cai and R.-G. Xiong, *J. Am. Chem. Soc.*, 2018, **140**, 8110-8113.
8. H. Peng, B. Zou, Y. Guo, Y. Xiao, R. Zhi, X. Fan, M. Zou and J. Wang, *J. Mater. Chem. C*, 2020, **8**, 6488-6495.
9. C. Li, X. Bai, Y. Guo and B. Zou, *ACS Omega*, 2019, **4**, 8039-8045.
10. X. Bai, H. Zhong, B. Chen, C. Chen, J. Han, R. Zeng and B. Zou, *J. Phys. Chem. C*, 2018, **122**, 3130-3137.
11. Y. Qin, P. Tao, L. Gao, P. She, S. Liu, X. Li, F. Li, H. Wang, Q. Zhao, Y. Miao and W. Huang, *Adv. Optical Mater.*, 2019, **7**. 1801160.
12. H. Y. Ye, Q. Zhou, X. Niu, W. Q. Liao, D. W. Fu, Y. Zhang, Y. M. You, J. Wang, Z. N. Chen and R. G. Xiong, *J. Am. Chem. Soc.*, 2015, **137**, 13148-13154.
13. L. Li, L. Li, Q. Li, Y. Shen, S. Pan and J. Pan, *Transit Met. Chem.*, 2020, **45**, 413-421.
14. V. Morad, I. Cherninkh, L. Pottschacher, Y. Shynkarenko, S. Yakunin and M. V. Kovalenko, *Chem. Mater.*, 2019, **31**, 10161-10169.
15. T. Jiang, W. Ma, H. Zhang, Y. Tian, G. Lin, W. Xiao, X. Yu, J. Qiu, X. Xu, Y. Yang and D. Ju, *Adv. Funct. Mater.*, 2021, 2009973.
16. B. Su, M. S. Molokeev and Z. Xia, *J. Mater. Chem. C*, 2019, **7**, 11220-11226.
17. C. Jiang, N. Zhong, C. Luo, H. Lin, Y. Zhang, H. Peng and C. G. Duan, *Chem. Commun.*, 2017, **53**, 5954-5957.
18. M. Li, J. Zhou, M. S. Molokeev, X. Jiang, Z. Lin, J. Zhao and Z. Xia, *Inorg. Chem.*, 2019, **58**, 13464-13470.
19. L. J. Xu, C. Z. Sun, H. Xiao, Y. Wu and Z. N. Chen, *Adv. Mater.*, 2017, **29**. 1605739.